

PROGRESS TOWARDS ADAPTIVE AIRCRAFT ENGINE NACELLES

L. da Rocha-Schmidt¹, A. Hermanutz¹, H. Baier¹, A. Seitz², J. Bijewitz²,
A. T. Isikveren², F. Scarpa³, G. Allegri³, C. Remillat³, E. Feuilleley³,
F. Majić⁴, C. O'Reilly⁴, G. Efrainsson⁴

¹ Technische Universität München, Germany, ² Bauhaus Luftfahrt e.V., München, Germany,
³ University of Bristol, UK, ⁴ Kungliga Tekniska Högskolan, Stockholm, Sweden

Abstract

Emissions and noise of aircraft engines have to be significantly further reduced and efficiency further increased in the future. One means is the improvement of airflow through the engine and especially so in its inlet region by proper shapes. Due to changes in the flight conditions, the optimal nacelle shape varies. It would thus be beneficial to be able to change the nacelle shape. Evaluations on system and engine levels including related flow simulations support the identification of proper shaping parameters. Initial concepts of possible morphing technologies are discussed as well.

1 Introduction and Overview

The objectives of reducing CO₂ and NO_x emissions as well as reducing community noise established in the ACARE Vision 2020 [1] have been defined at even more stringent levels in the Flightpath 2050 document [2]. For example, a reduction of perceived noise of 65% and of CO₂ emissions of 75% have been adopted. In order to achieve these longer term goals, possible measures are, amongst others, further improvement of the airflow within the engine and especially at its inlet. Because of the different aircraft flight conditions such as climb and cruise, flow conditions also change. This then calls for adaptive or morphing geometries of the nacelle. Initial investigations of such morphing nacelles are carried out in the study MorphElle funded by the European Commission. In this study, considerations on system and engine level together with related simulation tools and especially also of proper morphing technologies

are investigated. Basic challenges of morphing technologies are the conflicting goals of allowing the required shape morphing by proper structural flexibility on the one side, and on the other side the ability to safely take the different loads and to satisfy further requirements. Though the aforementioned challenge also exists in other areas of morphing aircraft, both the means of evaluation and assessment as well as those of related technologies are to be specifically related to aircraft engines and their nacelles. This then calls for concepts providing high material and structural flexibility in certain kinematic degrees of freedom, with sufficient strength and stiffness in those degrees of freedom where higher loads are to be taken.

In order to cover the aspects ranging from system over engine level to morphing technologies and related assessment and simulation methods, a study team has been established coordinated by Technical University Munich (TUM, Germany), with partners from University of Bristol (United Kingdom), the Royal Institute of Technology (KTH, Sweden) and Bauhaus Luftfahrt e.V. (Germany). This study team will be also advised by a Joint Technology Advisory Committee (JTAC) being composed of major European players in the field of aircraft engines.

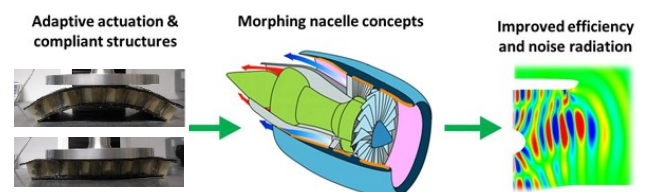


Fig. 1: Basic study goals of MorphElle

The basic study goals together with main approaches are briefly highlighted in Fig. 1. Though there are many different geometric parameters which can be chosen as morphing candidates to achieve the overall goals, those related to the inlet region have been selected as a priority. Some exemplary concepts are outlined in Fig. 2. Loosely speaking, the inlet has to properly adjust the airflow from outside to the entry of the fan and/or compressor with high mass flow and highest achievable pressure. Because of the different flight conditions, the inlet should be “thin” at cruise condition with higher Mach numbers, and somehow “round” together with possibly modified angles of attack to avoid flow separation during climb or at cross winds. Proper internal contouring maximizes inlet pressure recovery, and upper lip augmentation will improve windmill conditions.

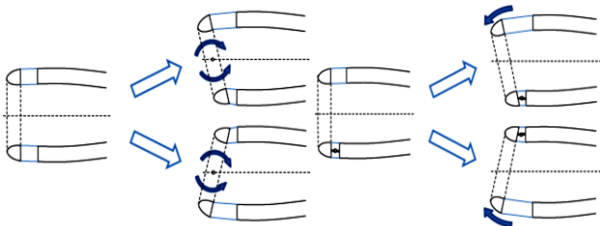


Fig. 2: Morphing lip concepts

It is obvious that a multidisciplinary design approach has to be chosen for defining such morphing nacelle systems. So based on established initial requirements and initial explorations, simulations of the air flow and resulting consequences for engine performance and immissions will support the identification of proper morphing measures. Morphing technologies will be derived from multidisciplinary engineering interfacing, material and structural simulations as well as materials and parts testing. Their geometrical performance will be demonstrated in a scaled test stand. The synthesis of results will allow to define a road map for further development in order to increase the TRL. More details and initial study results are presented in the following chapters.

2 Reference System Definition and Technology Benchmarking Approach

In order to define reference nacelles for this study, an in-service reference aircraft configuration (year 2000) as well as a projected design for the year 2025+ are defined. The according nacelles are used for design, simulation and performance benchmarking.

2.1 Identification of aircraft top level requirements for the year 2025+ technology reference

For the introduction of morphing nacelle technology into the commercial air transport market, the twin-engine wide-body aircraft market segment is considered most promising since medium-to-long application is expected to particularly benefit from improved efficiency and the resulting cascade effects of propulsion system and aircraft design. Further substantiating the selection of the wide-body market segment, an analysis of data on the worldwide air transport fuel burn [3] versus stage length reveals the significant impact of mid-to-long range operations on total fleet fuel consumption. For the subsequent determination of aircraft range requirements, Official Airline Guide (OAG) data for the year 2012 were used [4]. The stage-length-specific market growth and corresponding impact on the expected numbers of installed seats by the year 2025+ were derived from recent forecasts published by Airbus [5], Boeing [6], ICAO [7] and Rolls Royce [8]. A brief specification of the MorphElle reference application is given in Tab. 1.

Tab. 1: Overview of important top level requirements for MorphElle 2025+ reference aircraft

Range	4800 nm
No. of PAX	340 in 2-Class
Airport Compatibility Limits	ICAO Code E
External Noise & Emission Goals (Ref. 2000)	CO ₂ -41% NO _x -82% Noise -53% (interpolated SRIA 2025)
Technology Freeze – EIS	2020 – 2025

As datum reference, i.e. representing a typical year 2000 in-service system, an Airbus A330-

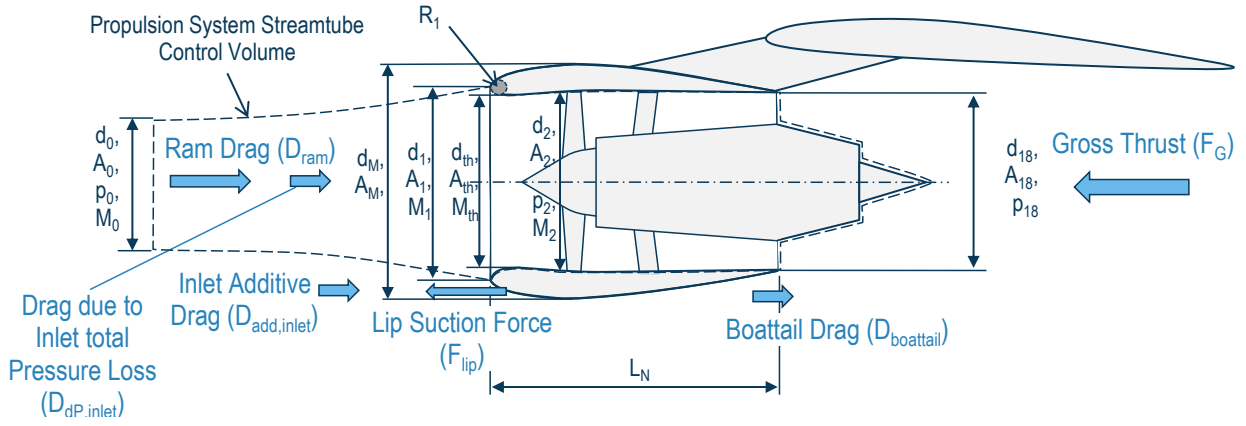


Fig 4: Control volume definition for thrust / drag book-keeping

300 [9] equipped with General Electric CF6-80E engines [10] was chosen as a baseline for the advanced technology benchmarking with respect to the goals defined by the European Strategic Research and Innovation Agenda (SRIA) [11].

2.2 Setup for Reference System Modelling and Technology Benchmarking

The final evaluation and benchmarking of the adaptive nacelle technology concepts investigated as part of the MorphElle Project will be based on an integrated fuel burn assessment performed at aircraft level. Therefore, the impact of active nacelle shaping on propulsion system performance parameters, nacelle drag, system weights and additional power demand emanating from the active [compliant] actuation system will be propagated to the vehicular level and thereby, cascade effects of power plant system and aircraft sizing captured in the final assessment. For the integrated aircraft assessment, the aircraft preliminary design environment APD 3.0 [12] suitably supplemented with a set of custom-developed high-end, semi-empirical methods is employed. Propulsion system conceptual design and performance synthesis is undertaken using the software GasTurbTM11 [13]. Therefore, a comprehensive set of typical design heuristics and cycle iteration strategies as well as appropriately predicted component efficiencies and pressure losses as presented in Reference [14] is incorporated. Turbo component off-design characteristics are based on GasTurbTM standard component maps [13]. For the mapping of the multidisciplinary effects on power plant

and aircraft design and performance associated with active shape changing of the nacelle, a consistent scheme for thrust and drag book-keeping is required. Serving this purpose, the control volume for power plant design and performance simulation is tailored according to the propulsion stream tube, as shown in Fig. 4.

All losses occurring inside the propulsion stream tube (cf. Fig. 4) are accounted as power plant internal losses. Propulsion system net thrust, F_N , accordingly yields:

$$F_N = F_G - D_{ram} - D_{dP,inlet} \quad (1)$$

where the engine gross thrust, F_G , readily includes losses due to jet shear flow on the core aft-body and nozzle plug. D_{ram} represents the engine ram drag, and, $D_{dP,inlet}$ denotes the drag due to engine intake total pressure loss. Aerodynamic forces acting outside of the propulsion stream tube are treated as aircraft drag shares. Therefore, nacelle total drag, D_{nac} , may be expressed as the sum of inlet spillage drag, $D_{spillage}$, and nacelle boattail drag, $D_{boattail}$:

$$D_{nac} = D_{spillage} + D_{boattail} = D_{add,inlet} - F_{lip} + D_{boattail} \quad (2)$$

where $D_{spillage}$ results from the typically counteracting forces of the pressure integral on the outer stream tube contour in front of the air intake, $D_{add,inlet}$, and the inlet lip suction force, F_{lip} .

In order to form a consistent basis and appropriate target settings for the technology studies to be performed as part of the MorphElle Project, basic nacelle geometric properties were

defined using the methods presented in references [14]. Intake geometric description is based on [15] and [16]. For flow path sizing conditions, intake pressure ratios, i.e. p_2/p_0 (cf. Fig. 4), were read from data given by [17] as a function of intake lip thickness and intake angle of attack. In order to estimate intake pressure recovery at engine part power, e.g. during cruise, characteristics presented by [18] were superimposed. Nozzle gross thrust and discharge were determined according to [14]. For the year 2025+ reference power plant, appropriately advanced cycle properties, i.e. pressure and temperature levels, as well as turbo component efficiency levels were assumed, and, customer offtakes mapped according to an all-electric aircraft systems architecture paradigm. The integrated power plant sizing and performance methods were validated for the CF6-80E1A2 engine using data published by Jane's [10]. In Tab. 2, an overview of central power plant characteristics of both, the year 2025+ technology reference and the year in-service baseline is given.

While both power plants feature Short Duct Separate Flow (SDSF) nacelle configurations, for the year 2025+ technology reference, a Geared Turbofan (GTF) power plant architecture is chosen in order to facilitate the significant increase of ByPass Ratio (BPR). As a result, the year 2025+ power plant features a 20% improved Thrust Specific Fuel Consumption (TSFC) at typical cruise conditions.

Tab. 2: Synopsis of important characteristics of year 2025+ reference power plant in comparison to year 2000 baseline model

	Y2000 Baseline	Y2025+ Reference
Architecture	2-spool, direct-drive turbofan	2-spool, geared turbofan
Stage Configuration	1-4-14-B-2-5	1-G-3-9-B-2-4
Nacelle Configuration	Short Duct Separate Flow	Short Duct Separate Flow
Fan Diameter	2.438 m	3.300 m
Engine Bypass Ratio	5	18
Cruise Spec. Fuel Consumption*	base	-20 %

*FL350, M0.8, ISA, 80% net thrust

Future work will focus on conducting sensitivity studies for potential morphing degrees of freedom. This includes appropriate mapping of nacelle drag characteristics and the resultant impact on power plant performance at relevant operating conditions. From the integrated aircraft performance environment, fuel burn trade factors will be derived suitable for the initial assessment of the investigated morphing pre-concepts.

3 Geometry and Computational Fluid Dynamics Model Description

To support the design process, a generic nacelle model is created. This geometry is used for both fluid dynamics simulations (CFD) and structural design and simulations (FEM). The model is kept highly parametric using splines and control points in order to represent the different reference nacelles and allow for sensitivity analysis through geometry variation.

3.1 Parametric Geometry Description

Movement of one point on the spline of inner contour changes the geometry of the inner contour of the nacelle. That point is represented by red dot in Fig. 5. Fixed points at fan plane and leading edge define the spline also. There are no other points between inlet and fan plane, which define the spline. The movable point is defined in cylindrical coordinate system by x-coordinate measured from inlet plane along engine centerline and r-coordinate measured from the engine centerline. The nacelle is axisymmetric around engine centerline.

The x-coordinate in the calculated configurations is changed from $0.2L_{DIFF}$ (L_{DIFF} – length of the diffuser) to $0.7L_{DIFF}$. The r-coordinate is changed from $0.85R_{FAN}$ (R_{FAN} – fan radius) to $1.05R_{FAN}$

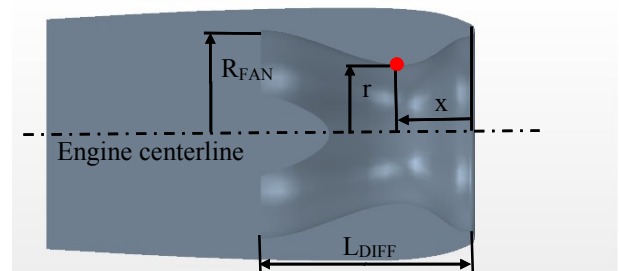


Fig. 5: Change of nacelle inner contour by moving point

3.2 Computational Fluid Dynamics Model

The numerical simulations were performed by solving the Reynolds Averaged Navier-Stokes (RANS) equations by control volume method. Turbulence is modeled by k- ϵ turbulence model employing the wall functions. The following parameters were used in all simulations:

- Free stream Mach number $Ma=0.367$
- Free stream temperature $T=276K$
- Engine mass flow $\dot{m}=698kg/s$
- Angle of attack $\alpha=16^\circ$

3.3 Preliminary CFD Simulation Results

The results of simulations are quantified and reported by two parameters [19]

- Coefficient of total pressure loss (CTPL)
- Surface standard deviation of normal velocity (σ) at fan plane

The coefficient of total pressure loss is defined as

$$CTPL = \frac{\bar{p}_{t,FAN} - \bar{p}_{t,\infty}}{0.5\rho_\infty V_\infty^2} \quad (3)$$

where $\bar{p}_{t,FAN}$ and $\bar{p}_{t,\infty}$ are mass flow averaged total pressures at fan plane and free stream respectively. ρ_∞ and V_∞ are density and velocity of the free stream respectively. σ is defined as

$$\sigma = \sqrt{\frac{\sum_n (V_{N,FAN} - V_{N,FAN,avg})^2 A_n}{\sum_n A_n}} \quad (4)$$

where $V_{N,FAN}$ and $V_{N,FAN,avg}$ are normal velocity at the fan plane and average normal velocity at the fan plane respectively. A_n is the area of the n^{th} surface element at the fan plane.

CTPL is an indicator of momentum losses from free stream to the fan plane and σ is an indicator of velocity non-uniformities at the fan plane.

In Fig. 6 the coefficient of total pressure loss is presented for different position of the moving point, which defines the contour of the inner contour of nacelle. Different curves represent families of different radial position of moving point, measured from engine centerline. Red curve with dots represent cases where radial

position of moving point is at $r=1.05 \cdot R_{FAN}$, blue curve with square represents case $r=0.95 \cdot R_{FAN}$ and black line with triangles represents $r=0.85 \cdot R_{FAN}$ where R_{FAN} is fan radius. On the abscissa the x position measured from the nacelle inlet along engine centerline is given. The x position is normalized by diffuser length L_{DIFF} .

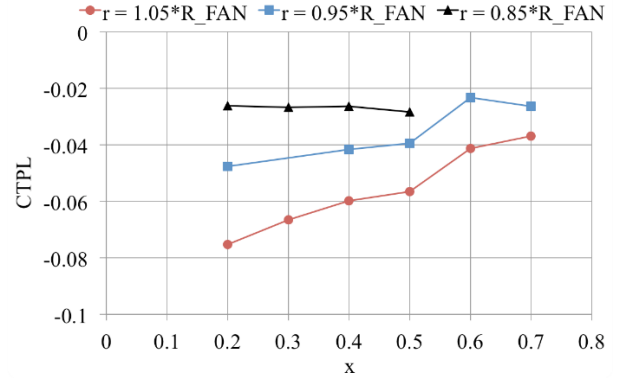


Fig. 6: Coefficient of total pressure loss for various nacelle contour geometries

Two curves ($r=0.95 \cdot R_{FAN}$ and $r=1.05 \cdot R_{FAN}$) show similar trend of CTPL by changing the x position of moving point. For those cases, the movement of the point closer to the fan plane decreases CTPL and is more beneficial. For the case $r=0.85 \cdot R_{FAN}$ the values of CTPL do not change considerably by changing x position from 0.2 to 0.5. For x positions $x=0.6$ and $x=0.7$ of the case $r=0.85 \cdot R_{FAN}$ the solution did not converge.

For the same x position of the moving point the radial position smaller than the fan radius gives less total pressure losses. Convergent-divergent type of channel ($r=0.85 \cdot R_{FAN}$ and $r=0.95 \cdot R_{FAN}$) is more beneficial than divergent-convergent type of channel ($r=1.05 \cdot R_{FAN}$). At divergent-convergent type the flow separation occurs over greater extent what can be visualized in Fig. 7 on lower side of nacelle inlet cross section.

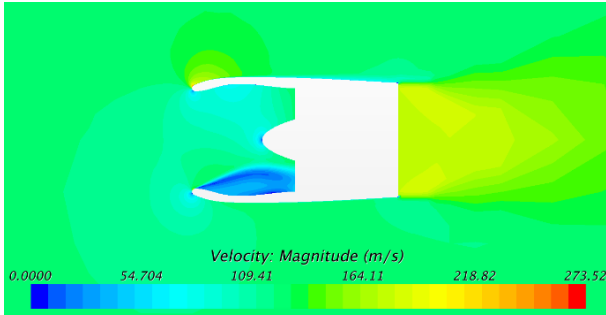


Fig. 7: Velocity magnitude in the vertical cross section plane

In Fig. 8 standard deviation of normal velocity at fan plane is presented. Each curve represents family of the same r coordinate of moving point for the range of x coordinates (normalized with length of diffuser) given on abscissa.

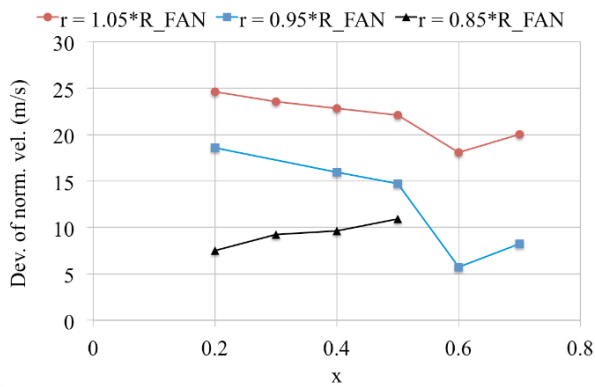


Fig. 8: Surface standard deviation of normal velocity at fan plane

The cases with $r = 1.05 \cdot R_{FAN}$ show the highest values of σ for all x positions of moving point, which is unfavorable with respect to state of the flow coming at the fan. Those are the cases with divergent-convergent type of inlet with the flow separation over great extent.

For the x positions of moving point close to the nacelle inlet the case with $r = 0.85 \cdot R_{FAN}$ shows the most favorable values of σ in comparison with other case. For x position $x = 0.6$ of the moving point, which is closer to fan, the most favorable case is $r = 0.95 \cdot R_{FAN}$.

The parametric model described in this section will be used in conjunction with structural simulations to support the design process.

4 Morphing and Actuation Concepts for Cellular Structures

In this section, a series of morphing structure concepts and their actuation is presented and evaluated. This is a first step in choosing valid concepts for the morphing nacelle.

Honeycomb cores are an integral part of modern acoustic duct liners, with the cellular structure often being structured in a multilayer configuration separated by a porous septum. Within the context of morphing technologies in aeroengine nacelles, it is therefore necessary to consider morphing cellular structures solutions to achieve both localized deformation of the duct sections, or even the possibility of adaptive scarfing of the nacelle lip (either upper or lower – see Fig. 9).

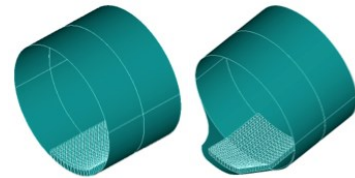


Fig. 9: Example of possible morphing scarfing through adaptive sandwich/honeycomb structure

Between the morphing cellular concepts developed during the last decade, it is possible to list the shape memory alloy morphing honeycombs [21][22] and the chiral configuration for the camber morphing of airfoil sections [23][24]. A significant example of morphing honeycomb technology is the distributed pneumatic actuation cell-by-cell by Vos and Barrett [25], which would allow in principle large actuation authority with precision control of the shape change. The main drawback of the pneumatic cellular structure proposed in [25] lies however on the extended pneumatic distributed system involved in the actuation, which tends to increase weight and decrease overall reliability because of the complexity of the system. It is therefore necessary to consider different actuations and structural configurations for the morphing cellular system adapted to the nacelle layout.

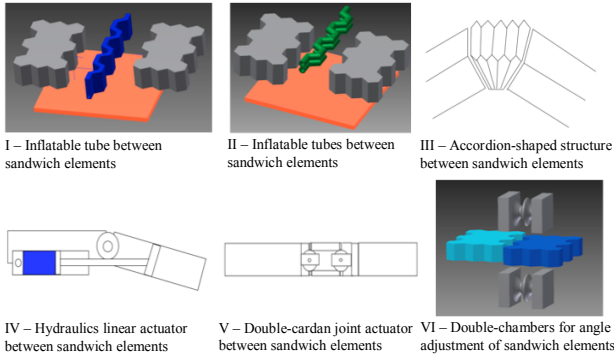


Fig. 10: Six different configurations evaluated for the pneumatic actuation of honeycomb sandwich panels.

We have evaluated six different design solutions to provide a pneumatic actuation within the honeycomb and sandwich duct liners, and reducing the numbers of actuators and power lines needed (Fig. 10). Single or double corrugated inflatable tubes can be placed between segments of sandwich panels, and the level of the input pressure would provide a translational effect to the single sandwich sections. The two concepts can also be adapted to work on a “smart-stick” actuation platform (Fig. 11), which has been developed by Berring et al. to provide a segmented rotational actuation similar to the one present in spider legs.

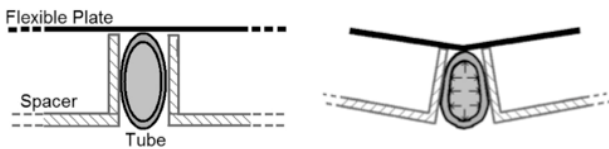


Fig. 11: “Smart-stick” principle: inflating the tubes produces the in-plane rotation of rigid segments connected by flexible skins [26].

Concept #3 involves the use of an accordion-type pneumatic connecting structure between the sandwich panels. Two design configurations (#4 and #5) are based on using classical linear hydraulic actuation units placed between the cellular structures –either a pneumatic linear actuator or a double cardan joint actuator. The final concept considered is represented by combinations of double pneumatic chambers located over the upper and lower skins of the sandwich panels. The application of differential pressure distributions between the two sets of chambers create a rotational movement, similar to the one of the smart-stick concept shown in Fig. 11.

The downselection of the final configuration amongst the 6 proposed has been carried out using a matrix decision analysis based on 11 parameters: cost, manufacturing, actuator max velocity, accuracy, power, robustness of the actuation, requirement of materials with adequate TRL, weight, complexity and maintenance issues. The different concepts have been classified from 1 (worst) to 6 (best). The double-cardan joint is considered with having the highest cost (1), while the accordion joint has been identified as being the less expensive (6). The weights have been identified first by ranking the parameters in a scale 1-10 (Tab. 3), then setting the weights to have $\sum_i w_i = 1$ with w_i being the weights of the parameters.

Tab. 3: Ranking of the parameters for the downselection process

Parameters	Rank
Cost	10
Manufacturing	3
Velocity	11
Accuracy/Precision	7
Power	9
Reliability	8
Durability/Strength	4
Materials	1
Weight	2
Complexity	5
Maintenance	6

A first decision matrix (that we will call **B**) is therefore created with 6 columns (the concepts) and 11 rows (parameters – see Tab. 4)

Tab. 4: First decision matrix of the design downselection

Parameters		I	II	III	IV	V	VI
Cost	0,02	5	4	6	2	1	3
Manufacturing	0,15	6	5	4	3	2	1
Velocity	0,01	4	3	6	1	2	5
Accuracy/Precision	0,06	4	5	1	2	3	6
Power	0,04	5	4	6	1	2	3
Reliability	0,05	4	6	1	2	3	5
Durability/Strength	0,12	2	3	1	5	6	4
Materials	0,20	5	6	3	2	1	4
Weight	0,17	6	5	4	2	1	3
Complexity	0,10	6	5	4	2	1	3
Maintenance	0,08	6	4	5	2	1	3
		5,02	4,85	3,33	2,46	2,02	3,31

The matrix **B** is first normalized, then decomposed, with each column multiplied by its weight w_i . The elements of the final matrix can then be plotted in either a linear or spider graphics to identify the best solution [27]. An alternative technique we have evaluated is based on the eigenvalue analysis of a rank-normalised version of the matrix B, and using the maximum eigenvalue to determine normalized weights and consistency index to obtain a final ranking matrix

[28]. The two techniques have given very similar results, also in terms of sensitivity and residuals.

The designs #1 and #2 (single and double tubes) provide similar overall performance, with the single tube being preferable in terms of weight, complexity and manufacturability (Fig. 12).

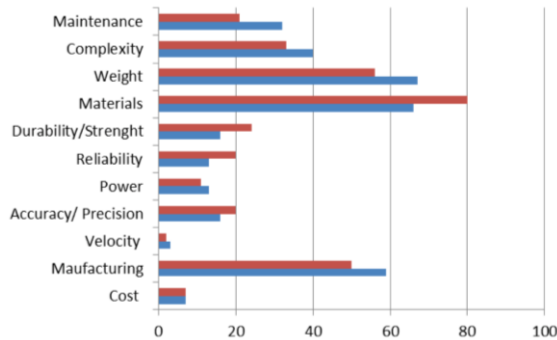


Fig. 12 Comparison between designs #1 and #2

The use of inflatable tubes in contact with finite sections of sandwich cores is however sensitive to relative sizes between core cells, dimensions and types of materials used for both core and tubes. To give a demonstration of this aspect, we have carried out a full-scale FE analysis on a section of honeycomb made out of PEEK core, and in contact with strengthened PVC-type tube (Fig. 13).

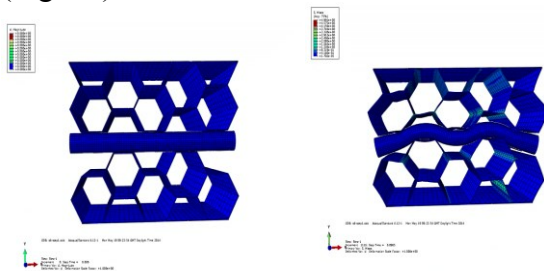


Fig. 13 FE simulation of maximum compressive strain when the tube is deflated between sandwich panel elements.

In large-scale cell sizes (6 mm X 6 mm), a maximum compressive strain of 16 % could be achieved between sandwich sections, with strong localized cell wall ribs deformation. The maximum Von Mises stresses would be still considerably lower than the equivalent yield stress of the PEEK polymer. The use of a design solution inspired to Fig. 11 would however limit significantly these scale effects in the deformation of the honeycombs, because it would be possible to place the tubes in contact

with a flat surface (“closed sandwich panel”), and therefore increase the contact area and the actuation authority of the system.

5 Shape Variable Inlet Lip Concept Description and Analysis

In this section, the concept of a morphing lip contour based on a pressurized shear compliant membrane skin is investigated in more detail since it proved to be very promising in preliminary evaluations.

This concept adapts the lip contour to different flow conditions of the flight envelope. Major goals of the lip contour change are to obtain a (more) laminar flow condition, avoid flow separations and decrease the loss of total pressure.

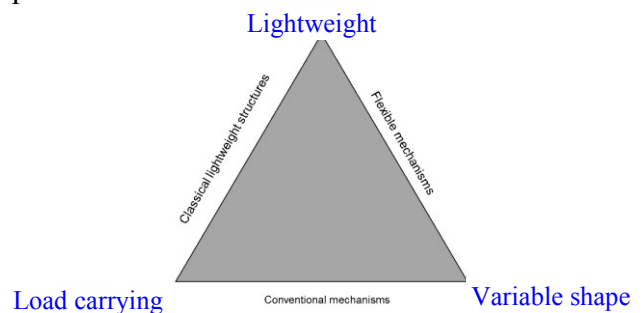


Fig. 14: Conflicting goals in morphing structures design

In order to solve the inherent goal conflict in morphing structures (see Fig. 14), the designs feature high stiffness in certain degrees of freedom (DOF) while keeping other DOF compliant.

The circular geometry of the nacelle makes morphing designs more challenging, compared to 2D aircraft wing morphing. Typical wing airfoil morphing concepts are difficult to transfer to the nacelle inlet due to the circumferential material strains that are induced when varying the diameter of parts of the nacelle, for example change of throat diameter. The presented concept of a morphing inlet lip uses a shear compliant metal mesh wire embedded in a silicone matrix to address this problem.

5.1 Morphing Inlet Lip Concept

The concept idea is based on a rigid part (tip of the lip) which is actuated translationally in axial direction (see Fig. 15).

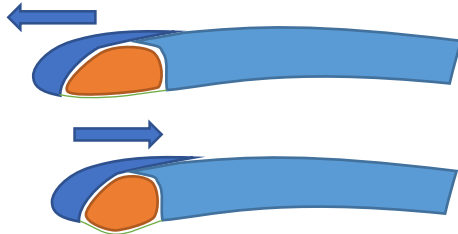


Fig. 15 Inlet lip morphing principle

The gap is covered with an elastic skin, which is internally pressurized by an air filled elastomeric tube. The main function of this tube is to support the elastic skin against the aerodynamic pressure. The static tube pressure has to be higher than the external aerodynamic pressure in order to keep the membrane skin under tension – and thus structurally stable – in all cases. The combination of rigid body translation and tube pressure defines the aerodynamic shape. A further condition that is derived from the stability criterion is a limitation of the membrane region to convex sections of the airfoil (like the lip). Concave parts of the inlet (further downstream) would not allow to keep tension stress in the membrane.

5.1.1 Morphing Inlet Lip – Skin Concept

Fig. 16 shows a closer view of the shear compliant metal wire membrane with a silicone matrix [20]. The material combination is stiff in wire direction to stand the aerodynamic loads and has a low shear stiffness to afford the shape change. The fiber orientation can be seen in Fig. 18.

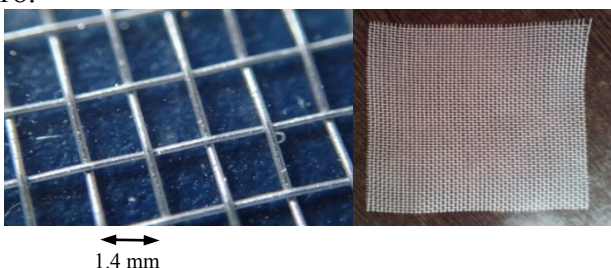


Fig. 16: Shear compliant morphing skin baseline (metal wire mesh with low stiffness silicone matrix)

5.2 Structural Analysis of the Morphing Lip Concept

5.2.1 Description of the Simulation Model

To investigate the structural behavior of the skin concept adapted to aero engine nacelles, a 10° segment of a generic nacelle is modelled to describe the geometry (see Fig. 17).

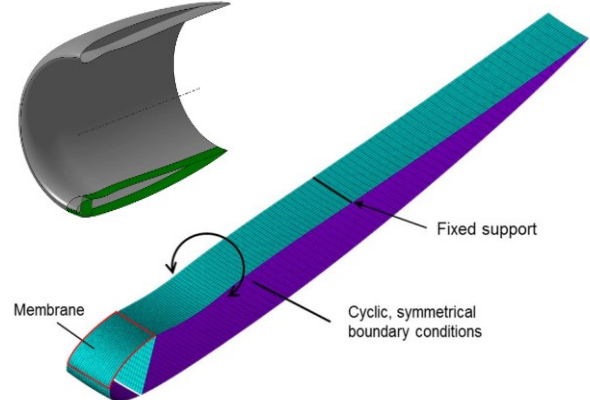


Fig. 17: Generic nacelle geometry model – 10° section used for structural FE model.

The membrane is modelled using shell FEM elements with a smeared approach of modelling the stiffness properties of the membrane skin. The flexible membrane is located in the front part of the airfoil with a +/- 45° wire angle (see Fig. 18). The membrane region can be modified parametrically.

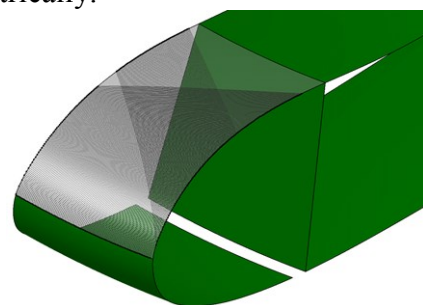


Fig. 18: Morphing skin (transparent) in the structural model

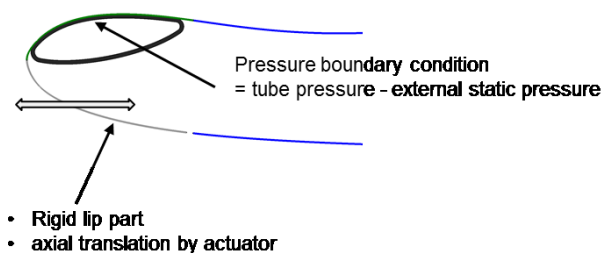


Fig. 19: Structural analysis pressure boundary condition and lip translation

The pressurized, air filled tube is represented via pressure loads on the membrane elements. The analyzed nacelle is axis symmetrical, therefore cyclic boundary conditions are applied by coupling the degrees of freedom of the side plane nodes in a cylindrical coordinate system.

In order to include stress stiffening effects of the membrane, the structure is analyzed using geometrically nonlinear Finite Element simulations.

5.2.2 Deformation Results of the Morphed Structure

The following results show achievable changes of the lip contour. Currently, shape change around the entire circumference is constant, but there is also the possibility to morph into different shapes between the top and the bottom part of the nacelle lip as hinted in Fig. 2.

As Fig. 21 shows, the axial translation is the main degree of freedom to influence the resulting lip shape. A further parameter is the static pressure of the tube, however this is limited by the aforementioned condition of always being higher than the external aerodynamic pressure.

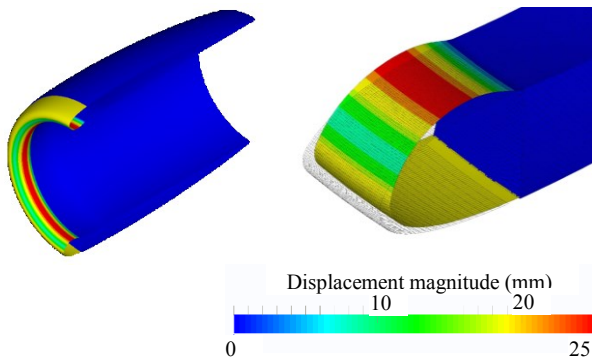


Fig. 20: Simulation results of deformed inlet lip shape under operational conditions

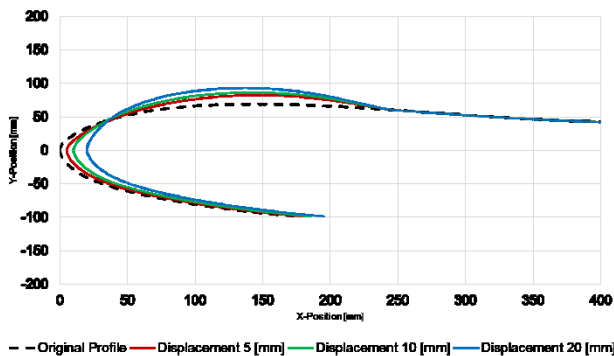


Fig. 21: Different achievable actuated lip shapes

In the next steps, the interaction with the aerodynamic simulations is planned, in order to include realistic external aerodynamic forces and to determine the benefits of the adapted aerodynamic shape. This will further be used to evaluate the high level benefits on the aircraft level.

6 Conclusion and Outlook

To investigate the concept of shape variability for aircraft engine nacelles, reference aircraft and nacelles have been defined for the year 2000 and 2025+. A parametric geometric nacelle model has been created and tested in several CFD simulations. It will be used in conjunction with FEM simulations to evaluate the developed morphing nacelles. General technological concepts have been developed for actuation, morphing structures, and skins. The pressurized morphing inlet lip concept has been investigated in detail. It appears to be capable of positively influencing the airflow in the nacelle and at the same valid in terms of manufacturing and actuation.

The multidisciplinary design process will be continued in order to finalize the exploration of the design space, evaluate possible solutions and refine the chosen designs. A hardware demonstrator of the preferred concept will be built and tested for actuation force, power requirements and achievable shapes.

7 References

- [1] ACARE. *European Aeronautics: A Vision for 2020*. European Commission, Belgium, 2001
- [2] European Commission. *Flightpath 2050 – Europe’s Vision for Aviation*. Belgium, 2011
- [3] Evers, C.J. et al. *AERO2k Global Aviation Emissions Inventories for 2002 and 2025*. website: http://aeronet.info/fileadmin/aeronet_files/links/documents/AERO2K_Global_Aviation_Emissions_Inventories_for_2002_and_2025.pdf, cited June 2013
- [4] Official Airline Guide (OAG). *Historical Data*. 2012
- [5] Airbus. *Global Market Forecast 2012-2031: Navigating the Future*. 2012
- [6] Boeing. *Current Market Outlook 2012-2031*. 2012
- [7] International Civil Aviation Organization (ICAO). *Outlook for Air Transport to the Year 2025*. 2007
- [8] Rolls Royce. *Market Outlook 2009 – Forecast 2009-2028*. 2009

- [9] Airbus. *A330 - Airplane Characteristics for Airport Planning*. France, 2005
- [10] M. Daly, B. Gunston. *IHS Jane's Aero Engines 2013/2014*. 2013
- [11] Advisory Council for Aviation Research and Innovation in Europe (ACARE). *Strategic Research and Innovation Agenda (SRIA) - Volume 1*, Brussels, 2012
- [12] PACE Aerospace Engineering and Information Technology GmbH. *Pacelab APD 3.0.0*. 2012
- [13] J. Kurzke. *GasTurb 11, compiled with Delphi 2007 on 27 January*, 2010
- [14] Seitz, A. *Advanced Methods for Propulsion System Integration in Aircraft Conceptual Design*, PhD Dissertation, Technische Universität München, 2012
- [15] Bräunling, W. *Flugzeugtriebwerke*, Springer-Verlag, Berlin Heidelberg, 2009
- [16] Farokhi, S. *Aircraft Propulsion*. John Wiley & Sons, 2009
- [17] Rick, H. *Gasturbinen und Flugantriebe - Grundlagen, Betriebsverhalten und Simulation*. Springer Vieweg, 2013
- [18] Mattingly, J. D., Heiser, W. H., Pratt, D. T. *Aircraft Engine Design*. 2nd Edition, AIAA Education Series, 2002
- [19] Manoj K G, Piyush G, Sunil P and Anil Dutt. *CFD analysis of performance characteristics of S-shaped diffusers with combined horizontal and vertical offsets*. Computers & Fluids, Vol. 40, No. 1, pp 280-290, 2011.
- [20] da Rocha-Schmidt, L, Baier, H. *Morphing Skins and Gap Covers for Aerodynamic Control Surfaces*. Deutscher Luft- und Raumfahrt-Kongress, Stuttgart, 2013
- [21] [1] Hassan MR, Scarpa F, Ruzzene M and Mohammed NA. Smart shape memory alloy chiral honeycombs. *Materials Science and Engineering: A*, Vol 481, pp 654-657, 2008
- [22] Hassan MR, Scarpa F and Mohammed NA. Shape memory alloys honeycomb: design and properties. *Smart Structures and Materials*, San Diego, CA, Vol. 557, paper number 5387, 2004.
- [23] Martin J, Heyder-Bruckner JJ, Remillat C, Scarpa F, Potter K and Ruzzene M. The hexachiral prismatic wingbox concept. *Physica Status Solidi (b)* Vol 245 (3), pp 570-577, 2008.
- [24] Bornengo D, Scarpa F and Remillat C. Evaluation of hexagonal chiral structure for morphing airfoil concept. *Proceedings of the Institution of Mechanical Engineers, Part G: Journal of Aerospace Engineering*, Vol 219(3), pp 185-192, 2004
- [25] Vos R. and Barrett R.M. Method and Apparatus for Pressure Adaptive Morphing Structure, *US Patent 2011/0038727 A1*, 2011
- [26] Berring J, Kianfar K, Lira C, Menon C, and Scarpa F. A smart hydraulic joint for future implementation in robotic structures. *Robotica* Vol 28(7), pp 1045-1056, 2010
- [27] Tam CM. *Decision Making and Operations Research Techniques for Construction Management*. City University of HK Press, 2007
- [28] Saaty TL. *Modern Nonlinear Equations*. Courier Dover Publications, 1981

8 Acknowledgements

This project (MorphElle, www.morphelle.eu) has received funding from the European Union's Seventh Framework Programme for research, technological development and demonstration under grant agreement no 341509.

The authors would like to thank Dr. Kay Plötner, Michael Schmidt and Clément Pernet for their valuable contributions in reference aircraft definition.

The help of Mr. Jian Sun in carrying out the FE simulations for the honeycomb with the inflatable tube is also acknowledged.

Copyright Statement

The authors confirm that they, and/or their company or organization, hold copyright on all of the original material included in this paper. The authors also confirm that they have obtained permission, from the copyright holder of any third party material included in this paper, to publish it as part of their paper. The authors confirm that they give permission, or have obtained permission from the copyright holder of this paper, for the publication and distribution of this paper as part of the ICAS 2014 proceedings or as individual off-prints from the proceedings.